Design of arbitrarily homogeneous permanent magnet systems for NMR and MRI: Theory and experimental developments of a simple portable magnet

Cedric Hugon, Francesca d'Amico, Guy Aubert, Dimitris Sakellariou

Design of arbitrarily homogeneous permanent magnet systems for NMR and MRI: Theory and experimental developments of a simple portable magnet

Cedric Hugon [a], Francesca D'Amico [b], Guy Aubert [c], Dimitris Sakellariou [a,*]

[a] *CEA, DSM, IRAMIS, SIS2M, LSDRM CEA Saclay F-91191 Gif-sur-Yvette, France*
[b] *CEA, DSM, IRAMIS, SIS2M CEA Saclay F-91191 Gif-sur-Yvette, France*
[c] *CEA, DSM, IRFU, CEA Saclay F-91191 Gif-sur-Yvette, France*

Starting from general results of magnetostatics, we give fundamental considerations on the design and characterization of permanent magnets for NMR based on harmonic analysis and symmetry. We then propose a simple geometry that takes advantage of some of these considerations and discuss the practical aspects of the assembly of a real magnet based on this geometry, involving the characterization of its elements, the optimization of the layout and the correction of residual inhomogeneities due to material and geometry imperfections. We report with this low-cost, light-weight magnet (100 euros and 1.8 kg including the aluminum frame) a field of 120 mT (5.1 MHz proton) with a 10 ppm natural homogeneity over a sphere of 1.5 mm in diameter.

1. Introduction

Portable NMR has been of interest since the early 1950s for NMR well-logging [1]. One of the first systems to go outside the laboratory was designed and fabricated by Varian and consisted of a polarizing coil which was shut off to let the spins evolve in the Earth's field [2]. Portable NMR did not draw much attention for a few decades thereafter due to the conflicting requirement for strong fields and portability. The development of new magnetic materials such as NdFeB and SmCo at the beginning of the 1980s [3] has brought new prospects for portable NMR. Previous materials (AlNiCo, ferrites, etc.) did not offer sufficient energy products to be suitable for NMR magnets. Halbach, sensing the possibilities offered by rare-earth magnets, developed his famous multipole structures around these new materials [4]. However, it was only in 1995 that the first truly portable NMR system was proposed, the NMR-MOUSE [5]. This system was among the first to offer the ability to perform NMR outside of a magnet, relaxing standard limitations on samples (e.g., size) applicable to NMR. Several other systems based on permanent magnets have been proposed for both, *ex situ* and *in situ* applications [6–14]. An extensive review on portable NMR by Blümich et al. is available for more details [11]. Although very promising NMR results have already been reported, the spectral resolution in a given sample volume obtained from permanent magnet systems cannot yet compete with what superconducting magnets currently offer. Part of the reason for the superior performance, is lying in long developments in magnetic field generation and control from electromagnets using Spherical Harmonics [15]. Even though this theory was very early transposed to permanent magnets by Aubert [16,17] in the context of 3D magnetic field control, only very recently, similar 2D and 3D analytical work has been published [8,18], giving rise to unilateral systems which use properly shaped polar pieces.

In this paper we propose a complete procedure for permanent magnet design, fabrication, characterization and shimming, which capitalizes on the spherical harmonic expansion. The theory is extensively presented and simple symmetry-based rules for magnet design are concluded. This approach for magnet design leads to theoretically perfectly controlled magnetic fields, up to arbitrary order, without the need of polar pieces. We also present a theoretical scheme for precise and direct measurement of the spherical harmonic expansion terms from real, and thus imperfect, magnets and we detail important issues dealing with folding. This tool allows us to pre-calculate the needed corrections for passive shimming, which has to be performed only once (in a way very similar to shimming the cryo-cooled shims in superconducting magnets) right after the magnet construction.

In practice, we have verified this procedure by creating and testing a simple magnet system with no pole pieces, that does not intend to achieve record performance. This test-bench is a

---

compact magnet assembly, based on small, inexpensive, magnetized cubes, that produces a longitudinal field in its center. Based on our theory, we developed and present algorithms to choose the layout of the cubes from 3D field measurements and sorting. Finally, we demonstrate passive shimming, using hard ferromagnetic elements in order to achieve the required compensations and we report NMR experiments.

2. Theory of spherical harmonic expansion (SHE)

2.1. Design of perfect permanent magnets

We describe in this section a general theory for the homogeneity of mobile permanent magnets, based on the spherical harmonic expansions (SHE) of the scalar potential and the magnetic field. We revise some well-known properties of this theory and then establish some symmetry-based rules for permanent magnets design.

In the case of NMR/MRI, the region of interest (RoI) is spherical and lies outside of the field sources region and one can define a magnetic pseudo-scalar potential ϕ^* such that:

$$\vec{B} = -\vec{\nabla}\Phi^* \tag{1}$$

This potential verifies the Laplace equation:

$$\Delta\Phi^* = 0 \tag{2}$$

The center of the sphere will be called the origin. We shall use spherical coordinates in the usual notation with r the distance from the origin, θ the inclination and ϕ the azimuth. The Laplace equation is separable in the spherical coordinate system and one can obtain a unique decomposition of the potential on the spherical harmonics base, centered on the origin. The general solution for the potential can then be written [19]:

$$\Phi^*(r, \theta, \phi) = \sum_{l=1}^{\infty} \sum_{m=-l}^{l} [A_{lm}r^l + B_{lm}r^{-(l+1)}]Y_{lm}(\theta, \phi), \tag{3}$$

where

$$Y_{lm} = \sqrt{\frac{2l+1}{4\pi}\frac{(l-m)!}{(l+m)!}}P_l^m(\cos\theta)e^{im\phi}. \tag{4}$$

One must remember that the potential exists only in empty areas of space. The space can therefore be divided in two areas where the potential exists: inside the biggest sphere centered on the origin that does not contain any source, and outside the smallest sphere centered on the origin that contains all the sources. Inside the former sphere, the potential can be expanded as:

$$\Phi^*(r, \theta, \phi) = \frac{1}{\mu_0} \sum_{n=1}^{\infty} r^n \left[Z_n P_n(\cos\theta) + \sum_{m=1}^{n} (X_n^m \cos m\phi + Y_n^m \sin m\phi)P_n^m(\cos\theta) \right], \tag{5}$$

where we call the Z_n terms axial terms and the X_n^m and Y_n^m terms skewed terms.

However, in NMR, we are interested in the magnetic field and not in the potential. As each component of the field satisfies the Laplace equation, it is possible to expand each component in the same way as the potential. However, the different terms are not the same. The longitudinal component of the magnetic field can be expanded as follows[1]:

$$B_z(r, \theta, \phi) = Zz_0 + \sum_{n=1}^{\infty} r^n \left[Zz_n P_n(\cos\theta) + \sum_{m=1}^{n} (Xz_n^m \cos m\phi + Yz_n^m \sin m\phi)P_n^m(\cos\theta) \right]. \tag{6}$$

The SHE expresses the variations of one component of the field at a time. However, the NMR frequency is proportional to the magnitude of the field, $B = |\vec{B}| = \sqrt{B_x^2 + B_y^2 + B_z^2}$. Hence, in order to see the small local variations of the field due to the chemical environment of the observed nucleus, a very homogeneous field is required. Yet we can remain concerned only about the main component of the field. This is stated in [15] but we shall prove it here.

Let the field at the center of the region of interest be $B_0 \vec{u_z}$. If we consider a small variation of the field, $\vec{b} = b_x \vec{u_x} + b_y \vec{u_y} + b_z \vec{u_z}$ with $b = \sqrt{b_x^2 + b_y^2 + b_z^2} \ll B_0$, we have for the magnitude of the total field:

$$B = \sqrt{(B_0 + b_z)^2 + b_x^2 + b_y^2},$$

or

$$B = B_0 \left[1 + \frac{b_z}{B_0} + O\left(\frac{b}{B_0}\right)^2 \right]. \tag{7}$$

Eq. (7) shows that the variations of the main component of the field come in first order while the other components start at the second order. As a result, we can restrict the study of homogeneity to the main component of the field. This main component may obviously be in any direction of space, but in NMR it is usually pointing along the z axis of the laboratory. This approximation is of course only valid in a region of space where the field variations are small compared to the main field. It is otherwise necessary to deal with the three components.

Eq. (6) shows that the homogeneity requirements correspond to an expansion of the field featuring the order 0 term only. This is not possible, but we can cancel as many terms as necessary to achieve the required homogeneity over a desired volume. As the variations induced by a term of order n scale as $\left(\frac{r}{r_0}\right)^n$, with r_0 being a reference radius smaller than the radius of the largest sphere containing no sources, the field inhomogeneities will be dominated by the term of lowest order. Thus, to achieve the desired homogeneity, the k first orders should be cancelled until $\left(\frac{r}{r_0}\right)^{k+1}$ is small enough. We shall now see how it is possible to cancel these terms through a systematic design of the magnet. Symmetries in the structure of the magnet may help tremendously this task. The symmetry of the magnet layout will reflect directly into the potential symmetries (it is indeed the potential that is really defined by placing magnetic pieces of specific geometries in space). It is hence necessary to consider the potential expansion before going to the field expansion.

The conversion between potential and field component expansion terms can be established analytically [15]. We can write, for example, for the B_z component[2]

$$Xz_n^m = -(n+m+1)X_{n+1}^m \quad \forall n \geqslant 1, 1 \leqslant m \leqslant n, \tag{8}$$

$$Yz_n^m = -(n+m+1)Y_{n+1}^m \quad \forall n \geqslant 1, 1 \leqslant m \leqslant n, \tag{9}$$

$$Zz_n = -(n+1)Z_{n+1} \quad \forall n \geqslant 0. \tag{10}$$

---

[1] The transverse components (B_x and B_y) would of course follow a similar expansion.

[2] It is also possible to obtain similar relations for the other components of the field but this goes beyond the focus of this paper.

It is straightforward to conclude that in order to obtain a homogeneous longitudinal field, one should find a source distribution that creates a potential for which the expansion contains only the Z_1 term. An n-fold rotational symmetry will remove the potential skewed terms up to order $n - 1$, the first non-zero skewed terms being then X_n^n and Y_n^n. Hence, the B_z skewed terms up to order $n - 2$ will be cancelled (the first non-zero term being at order $n - 1$). Once skewed terms have been zeroed, the remaining axial terms must be taken care of. Another helpful symmetry is then the planar antisymmetry with respect to xOy, which will leave only odd axial terms in the potential, hence leaving only even terms in the expansion of B_z.[3] It is then possible to arbitrarily cancel p axial orders by choosing the proper dimensions and layout of $p + 1$ independent sources featuring the n-fold rotational symmetry. The optimization of these magnet elements becomes quickly difficult and prohibitively long if not supported by analytical formulas of the expansion terms. We have derived such analytical formulas for different source shapes (cylinders, rings and trapezoids), which relate the spherical harmonic expansion coefficients to selected relevant geometric parameters. Based on these equations, numerical optimization provides the ideal parameters for a type of geometry and the desired field homogeneity.

2.2. Direct measurement of the SHE terms

Using the previously described theory, theoretically perfect magnets can be designed having an arbitrary field profile. In practice though, many imperfections (positioning, magnetization heterogeneities from fabrication, demagnetization, etc.), will contribute to an imperfect magnetic field. In the context of electromagnets, a field mapping approach in view of the computation of the SHE terms [15] offered possibilities for efficient shimming. However, in the literature no detailed discussion of critical issues of this technique related to folding have been given in the past. In addition, to the best of our knowledge this technique has not been applied to mobile permanent magnets for NMR until now.

The field of a magnet can be characterized in many different ways, the most straightforward of which is to map the field on a Cartesian grid with an appropriate detector (Hall or NMR probe). It is also possible to use the gradient shimming technique which relies on the use of external gradients to map the field everywhere in the volume of interest [20]. This technique however depends highly on the quality of the gradients used to map the field and requires the external gradients to be stronger than the field variations throughout the volume of interest. Furthermore, a field appearing constant with this technique only reflects the linearity of the gradients: once the gradients are removed, the field features the imperfections of the gradients. Some quality factor can be defined based on the different measurement points in order to assess the quality of the field. However, it is difficult to explicitly qualify the variations and compare one profile with another one based solely on such a quality factor. Spectral analysis, or the decomposition of a function onto an orthonormal basis is probably one of the most efficient ways of qualifying that function and comparing it to another one. The spherical harmonic expansion is in that sense a very convenient tool and has been extensively used in magnet design and characterization [15].

Field measurements can only be done in a finite number of discrete locations and the operation of retrieving the expansion terms from such measurements corresponds to a polynomial interpolation. This raises the issues of choosing the appropriate measurement points and aliasing. The following theoretical description of

aliasing in the context of field plotting is largely inspired from the numerous literature available on the topic of interpolation and sampling points choice (see for example [21,22]).

In order to perform the right measurements and carry the right interpolation, it is important to define the number of terms to retrieve and this cannot be dealt with without having aliasing in mind. If we sample a polynomial P in n points x_i, we can define the polynomial Π such that

$$\Pi(x) = (x - x_1)(x - x_2) \cdots (x - x_i) \cdots (x - x_n) \qquad (11)$$

As a result, if we divide P by Π, we obtain a quotient Q and a remainder R:

$$P(x) = Q(x)\Pi(x) + R(x) \qquad (12)$$

For the sample point x_i, we obtain

$$P(x_i) = R(x_i) \qquad (13)$$

and it is not possible to make the difference between P and R. We shall call Π the sampling polynomial.

For example, let the field variation V to be measured of the form

$$V(r, x) = Z_0 P_0(x) + \left(\frac{r}{r_0}\right) Z_1 P_1(x) + \left(\frac{r}{r_0}\right)^2 Z_2 P_2(x) + \left(\frac{r}{r_0}\right)^3 Z_3 P_3(x)$$
$$+ \left(\frac{r}{r_0}\right)^4 Z_4 P_4(x) + \left(\frac{r}{r_0}\right)^5 Z_5 P_5(x)$$

with $x = \cos\theta$. Let us sample that field variation in three points lying on the sphere of radius $r < r_0$ and corresponding to $\cos\theta = \frac{1}{2}, 0, -\frac{1}{2}$. The sampling polynomial is hence defined as

$$\Pi(x) = x\left(x - \frac{1}{2}\right)\left(x + \frac{1}{2}\right).$$

One then finds out that R, as defined above, can be written as

$$R(r, x) = \left[Z_0 - \frac{49}{96}\left(\frac{r}{r_0}\right)^4 Z_4\right] P_0(x) + \frac{r}{r_0}\left[Z_1 - \frac{7}{8}\left(\frac{r}{r_0}\right)^2 Z_3\right.$$
$$\left. + \frac{23}{128}\left(\frac{r}{r_0}\right)^4 Z_5\right] P_1(x) + \left(\frac{r}{r_0}\right)^2 \left[Z_2 - \frac{85}{48}\left(\frac{r}{r_0}\right)^2 Z_4\right] P_2(x).$$

If we write the terms calculated from sampling (primed terms) as a function of the real terms (unprimed terms), we obtain

$$Z_0' = Z_0 - \frac{49}{96}\left(\frac{r}{r_0}\right)^4 Z_4$$

$$Z_1' = Z_1 - \frac{7}{8}\left(\frac{r}{r_0}\right)^2 Z_3 + \frac{23}{128}\left(\frac{r}{r_0}\right)^4 Z_5$$

$$Z_2' = Z_2 - \frac{85}{48}\left(\frac{r}{r_0}\right)^2 Z_4.$$

This demonstrates that for insufficient, non-optimized sampling points, the higher order terms of the expansion fold into the evaluated terms. This is due to the fact that we limit the interpolation to three terms while the actual field variation features six of them. Here, we want to emphasize that this problem is always present when performing field profiling. The measurement requires to set a finite number of measurement points and to truncate the expansion. The actual field expansion always features more terms than we fit. However, the expansion usually converges and there exists an order above which terms can be neglected and will not affect the extraction of the coefficients. The number of necessary terms depends on the system producing the field. Hence, one should assess first what is the spectral content likely to be found, based on the geometry and imperfection sources. The validity of the choice

---

[3] This symmetry cannot be achieved in the case of *ex situ* systems, where magnetic sources are allowed only on one side of the RoI.

of the necessary number of points should later be checked by verifying the stability of the interpolation while varying the number of measurement points or the number of measured terms.

After the number of measurement points is chosen, it is necessary to decide where these points should be. It is a well-known property of the solutions of the Laplace equations, that if one knows the field on a closed surface containing no sources, it is possible to compute the field anywhere inside this surface. Hence, it is possible to retrieve the inner spherical harmonic expansion from measurements on a closed surface that does not contain any source. The sphere is the most adapted geometry and the radius of measurement should contain the entire volume of interest (inaccuracies resulting from the measurement errors are amplified by extrapolation outside the measurement sphere).

However, we want to stress that the effect of aliasing depends in addition on the radius of measurement. Therefore, the increase of the radius of measurement must be done with care as aliasing may corrupt the retrieved terms, resulting in potentially larger errors than measurement errors. Hence, one may need to compute more terms (and use more points).

There are many ways of sampling the surface of the measurement sphere. We shall discuss here a well-known [15] simple and straightforward one, though not optimal. This sampling scheme offers ease for calculation and practical measurement. It is a combination of an equidistant distribution in ϕ so that the m orders can be calculated through a simple Fourier transform and an equidistant distribution in θ in order to get the n orders through a simple fit. It is obvious that one needs at least $2M + 1$ points to obtain all orders m up to M and at least $N + 1$ different θ in order to retrieve the n orders up to N. The even sampling in θ insures that the lower orders are the least affected by aliasing, making it easier to obtain a reliable measurement (through increase of measurement points). This sampling scheme necessitates much more points than necessary as $2M + 1$ points are taken for each θ. For θ close to 0 or π, numerous points in ϕ are useless. It is possible to determine an optimal sampling scheme, however, the definition of such a sampling grid goes beyond the scope of this paper.

3. A simple practical example

This section describes a simple magnet system based on the previously exposed SHE framework. A short discussion of well-known imperfections of permanent magnets is given and we present an original methodology to measure with good precision the magnetic moment of cubes (amplitude and orientation). A short discussion of a screening procedure based on these measurements follows. The concept of screening parts has been applied for a long time but the given procedure is original. The ability to simulate quantitatively the field variations based on the cube measurements is demonstrated for the first time.

3.1. Magnet design

Based on the preceding theory, we can analyze a very simple magnet structure that creates a longitudinal field (i.e. B_z in the notation of the preceding section). This magnet structure was originally invented by Aubert [16] and preliminary developments were recently discussed [23]. We will summarize the theoretical analysis and focus on practical aspects. The theoretical structure is divided in rings which have a cylindrical symmetry with a number of segments. We chose to use two rings for which the segments consisted in cubes arranged cylindrically and anti-symmetrically, as shown on Fig. 1. Fourty-eight cubes having a side of 12 mm were used and the diameter of the bore of the magnet was 52 mm. Assuming the cubes are all exactly the same and feature homoge-
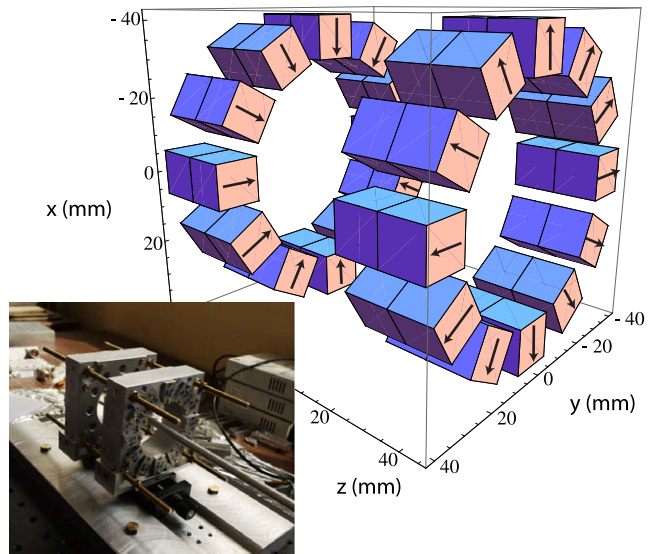

Fig. 1. Basic layout of the magnet system. It consists of two rings of magnet blocks that are radially magnetized. The combination of these rings creates a longitudinal field at the center of the system and confines the field in the structure. The magnetization of each cube is shown as an arrow on the side. The photograph at the bottom left shows the final implementation of the cubes in aluminum mounts set on translation stages for adjustments.

neous magnetization, the cylindrical arrangement of 12 cubes provides a 12-fold rotational symmetry, cancelling all field skewed terms until the 11th order, while the antisymmetric arrangement of the two rings provides the cancellation of every odd axial term. The use of two rings allowed the cancellation of one extra axial term through the use of the appropriate gap (about 42.122 mm). A photograph of the assembly is shown on Fig. 1. The two rings of cubes are supported by machined aluminum mounts mounted on linear translation stages (Owis brand, model VT 65-Z-FGS, non-magnetic version) in order to adjust the gap between the two rings. Bracings maintain the gap once the magnet is adjusted and removed from the linear stages. This magnet, once set up properly, should offer a homogeneous field up to order 4. This corresponds to a homogeneity of 15 ppm over a 3 mm DSV. Fig. 2 provides a view of the field variations for this theoretical model (simulations are done using exact cube geometry). Making an axial magnetic field is usually less efficient than making a transverse one, using the configuration of Halbach. In our case, with the same number of cubes representing 630 g of magnetic material, one could generate a transverse magnetic field of 190 mT with the same bore radius. The homogeneity of this magnet would be 15 ppm in 3 mm DSV. Using axially magnetized blocs would lead to even worse efficiency compared to the Aubert or Halbach configurations. In our case the field generated by such a configuration is 90 mT, with a homogeneity of 26 ppm in 3 mm DSV.

It is straightforward to estimate the effect of position errors of the different magnet parts from the theoretical calculations. These estimations indicate the positioning of the magnets must be very precise. For example, an error of 0.05 mm on the gap between the rings induces the rise of 15 more ppm of inhomogeneity on the same diameter, due to the increase of Zz_2.

3.2. Material imperfections

The cubes constituting the magnet assembly are not perfect and feature a distribution of magnetization amplitude and orientation from one to another. Geometrical tolerances are also a source of imperfections such as imperfections in the geometry, the location
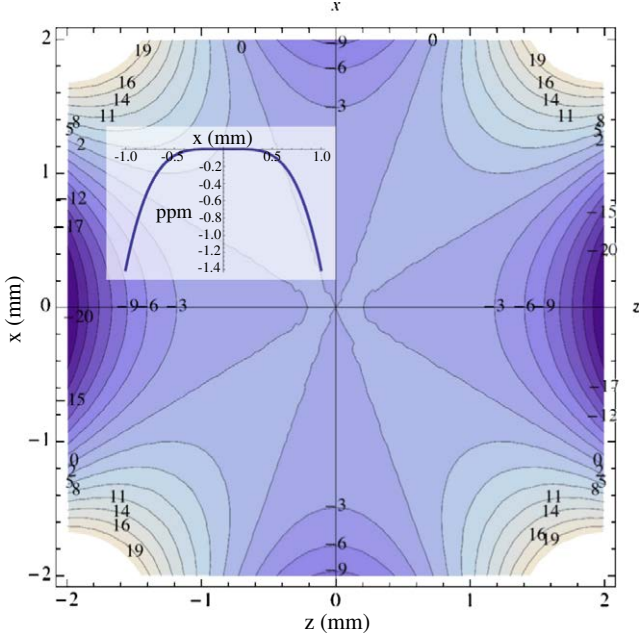
Fig. 2. Contour plot of B_z in the *XZ* plane, as the theoretical magnet should produce. One can notice that the variations are dominated by the order 4, and are limited to about 40 ppm over a sphere of 4 mm diameter. Levels are in ppm. The plot in the white box shows the field variation in ppm for $z = 0$ with x varying. A homogeneity below 0.2 ppm could be achieved in a volume of 1 mm^3.

and the orientation of each cube and then in the orientation and location of each ring. In most cases, the primary source of imperfections in the field are the distribution of magnetization from one cube to another and the errors on the orientation and location of the rings.

Furthermore, the magnetization is not homogeneous throughout each cube. This is caused by the (imperfect) fabrication processes and the demagnetizing fields due to the geometry of the magnet which also induce an inhomogeneous magnetization by setting a different working point throughout the magnet. The demagnetization of a part can be simulated by iterative algorithms such as the one in Radia, a software proposed by the ESRF [24]. However, such simulations remain not precise enough for magnetic resonance (0.5 percent compared to experimental results), due to the little knowledge we have of the material behavior and of its history. Such methods are at best a good way to help refine the assembly of a magnet. One must be prepared in the end to significantly shim the magnet to obtain performance suitable for NMR.

3.3. Magnetic measurement of magnet pieces

Good knowledge of the magnetic properties of each piece is necessary in order to achieve high performance and more precise simulations. It is extremely difficult to retrieve the magnetization distribution of the magnet part but one can measure with a good precision (but poor accuracy) its average magnetization. This can be done by assuming a dipolar approximation of the magnet part [23]. Several methods can then be used, either based on Hall probes [25] or on flux coils (see for example Section 5.2 in [26]). The dipolar approximation is a very good one for any geometry as long as one measures the field sufficiently far away from the part. For a cube, the sensor should be located at least at a distance five times the size of the cube. However it was not possible for us to perform the measurements at a distance sufficiently remote to safely assume a dipolar behavior.

It is possible to refine the model used to get the average magnetization when a 3D field map of the field can be obtained. Using the same measurement scheme as in our moment measurement, we can use analytical formulas for the field generated by a parallelepiped [27]. One can indeed write the field generated by a parallelepiped of dimensions 2a, 2b and 2c, magnetized along the z direction (Fig. 3) as:

$$B_x^z(x,y,z,a,b,c) = \frac{M_z}{4\pi} \ln \left[\frac{y+b+\sqrt{(y+b)^2+(x-a)^2+(z-c)^2}}{y-b+\sqrt{(y-b)^2+(x-a)^2+(z-c)^2}} \right.$$
$$\cdot \frac{y-b+\sqrt{(y-b)^2+(x+a)^2+(z-c)^2}}{y+b+\sqrt{(y+b)^2+(x+a)^2+(z-c)^2}}$$
$$\cdot \frac{y-b+\sqrt{(y-b)^2+(x-a)^2+(z+c)^2}}{y+b+\sqrt{(y+b)^2+(x-a)^2+(z+c)^2}}$$
$$\left. \cdot \frac{y+b+\sqrt{(y+b)^2+(x+a)^2+(z+c)^2}}{y-b+\sqrt{(y-b)^2+(x+a)^2+(z+c)^2}} \right],$$

$$(14)$$

$$B_y^z(x,y,z,a,b,c) = \frac{M_z}{4\pi} \ln \left[\frac{x+a+\sqrt{(y-b)^2+(x+a)^2+(z-c)^2}}{x-a+\sqrt{(y-b)^2+(x-a)^2+(z-c)^2}} \right.$$
$$\cdot \frac{x-a+\sqrt{(y+b)^2+(x-a)^2+(z-c)^2}}{x+a+\sqrt{(y+b)^2+(x+a)^2+(z-c)^2}}$$
$$\cdot \frac{x-a+\sqrt{(y-b)^2+(x-a)^2+(z+c)^2}}{x+a+\sqrt{(y-b)^2+(x+a)^2+(z+c)^2}}$$
$$\left. \cdot \frac{x+a+\sqrt{(y+b)^2+(x+a)^2+(z+c)^2}}{x-a+\sqrt{(y+b)^2+(x-a)^2+(z+c)^2}} \right],$$

$$(15)$$

$$B_z^z(x,y,z,a,b,c) = \frac{M_z}{4\pi} \left[\arctan \frac{(x+a)(y+b)}{(z-c)\sqrt{(y+b)^2+(x+a)^2+(z-c)^2}} \right.$$
$$- \arctan \frac{(x+a)(y+b)}{(z+c)\sqrt{(y+b)^2+(x+a)^2+(z+c)^2}}$$
$$+ \arctan \frac{(x-a)(y-b)}{(z-c)\sqrt{(y-b)^2+(x-a)^2+(z-c)^2}}$$
$$- \arctan \frac{(x-a)(y-b)}{(z+c)\sqrt{(y-b)^2+(x-a)^2+(z+c)^2}}$$
$$- \arctan \frac{(x+a)(y-b)}{(z-c)\sqrt{(y-b)^2+(x+a)^2+(z-c)^2}}$$
$$+ \arctan \frac{(x+a)(y-b)}{(z+c)\sqrt{(y-b)^2+(x+a)^2+(z+c)^2}}$$
$$- \arctan \frac{(x-a)(y+b)}{(z-c)\sqrt{(y+b)^2+(x-a)^2+(z-c)^2}}$$
$$\left. + \arctan \frac{(x-a)(y+b)}{(z+c)\sqrt{(y+b)^2+(x-a)^2+(z+c)^2}} \right].$$
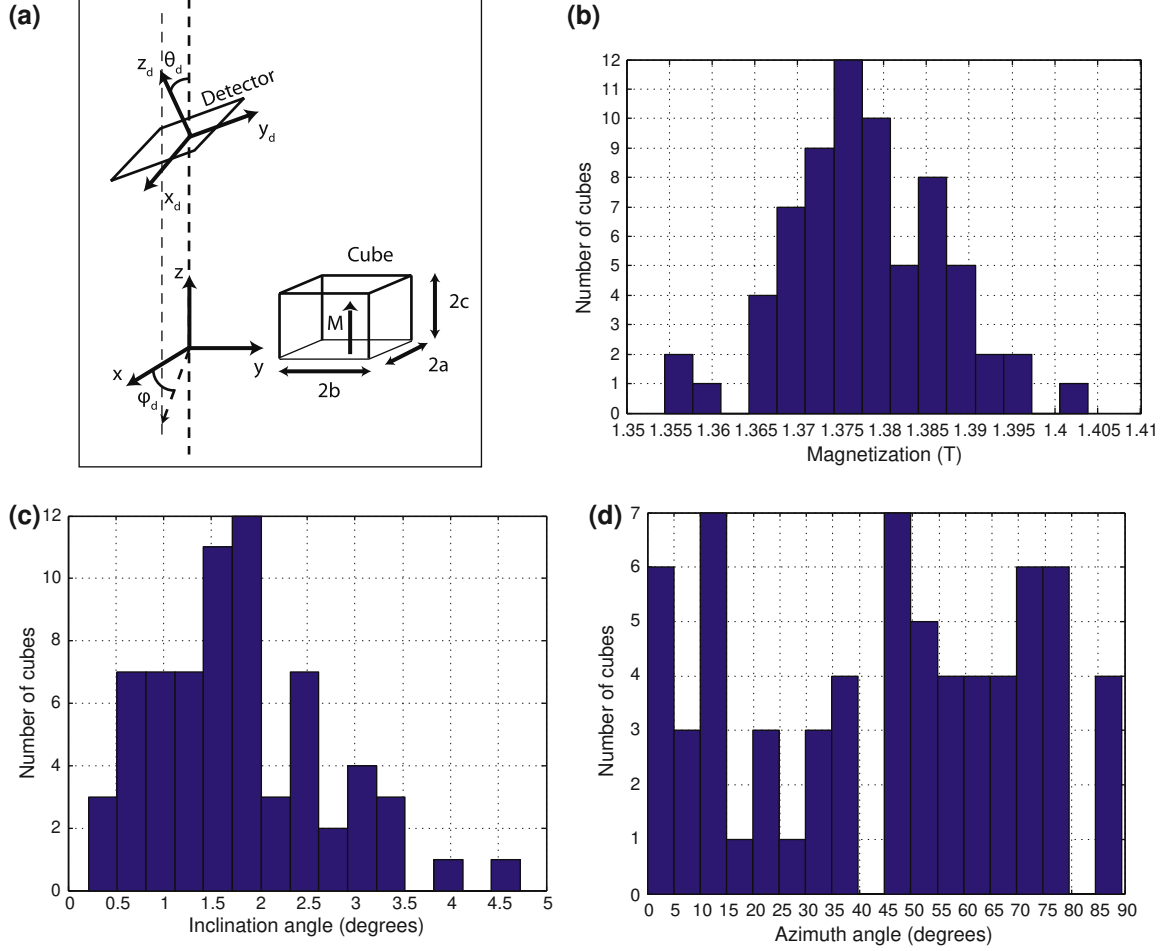
$$(16)$$

Fig. 3. Measurements of the magnetization magnitude for an ensemble of 68 cubes. Measurements are performed by placing sequentially the north pole and the south pole of each cube along the positive Z axis of the laboratory frame. (a) Definition of the different geometrical quantities considered for the measurement of the magnetization of a cube. The parallelepiped is shown with sides $2a$, $2b$ and $2c$ referring to the a, b, and c of Eqs. (14)–(16). The detector attitude relative to the reference frame of the parallelepiped is shown with the different relevant angles (θ_d and ϕ_d found in Eq. (20)). (b) Histogram of the magnetization amplitude The average magnetization is 1.38 T and the standard deviation is 0.01 T. (c) Histogram of the magnetization inclination. Average inclination is 1.8° and the standard deviation is 0.9°. (d) Histogram of the magnetization azimuth. Mean value and standard deviation are irrelevant. The azimuth can always be reduced to a value between 0° and 90° as the cube can be rotated by quarter of turns without changing the geometry. The most relevant parameters are here the amplitude and the inclination which show significant spreads.

We have developed Eqs. (14)–(16) further in order to use them for cube measurements. The field generated by the same parallelepiped magnetized along x or y satisfies the same equations after the proper transformation of coordinates and permutations of a, b and c. We shall define the following notations to refer to the field generated by the different magnetization coordinates:

$$P_\alpha^X(x,y,z,a,b,c) = \frac{1}{M_z}B_\alpha^Z(-z,y,x,c,b,a),$$

$$P_\alpha^Y(x,y,z,a,b,c) = \frac{1}{M_z}B_\alpha^Z(x,-z,y,a,c,b),$$ (17)

$$P_\alpha^Z(x,y,z,a,b,c) = \frac{1}{M_z}B_\alpha^Z(x,y,z,a,b,c),$$

where α can be x, y or z. Using this notation, one can express any component of the field generated by the parallelepiped through the following equations:

$$B_x(x,y,z,a,b,c) = M_x P_x^X(x,y,z,a,b,c) + M_y P_x^Y(x,y,z,a,b,c) + M_z P_x^Z(x,y,z,a,b,c),$$
$$B_y(x,y,z,a,b,c) = M_x P_y^X(x,y,z,a,b,c) + M_y P_z^Y(x,y,z,a,b,c) + M_z P_y^Z(x,y,z,a,b,c),$$
$$B_z(x,y,z,a,b,c) = -M_x P_x^X(x,y,z,a,b,c) - M_y P_y^Y(x,y,z,a,b,c) + M_z P_z^Z(x,y,z,a,b,c).$$ (18)

This can be summarized in matrix formalism for any component α of the field as

$$B_\alpha = [\,\delta_{x,\alpha} \quad \delta_{y,\alpha} \quad \delta_{z,\alpha}\,]\begin{bmatrix} P_z^X & P_x^Y & P_x^Z \\ P_y^X & P_z^Y & P_y^Z \\ -P_x^X & -P_y^Y & P_z^Z \end{bmatrix}\begin{bmatrix} M_x \\ M_y \\ M_z \end{bmatrix},$$ (19)

where $\delta_{\beta,\alpha}$ = 1 if $\alpha = \beta$ and zero otherwise.

It can be noticed that only one component of the field is required to retrieve the three components of the magnetization if one obtains several measurements in different locations. Using only one component of the field solves the issue of measuring the three components of the field at the exact same location. We will now remain concerned with the z component of the field, which is measured in several points. One must be careful during the measurement of one component of the field to have negligible orthogonal components in the field in order to avoid errors due to the planar field effect [25].

It is very important to take into account the possible misalignment of the cube's reference frame with the translation's and detector's ones. In our context, we assume the translation reference frame is aligned with the cubes reference frame by construction. However, the position of the detector and its orientation are not very well known. The detector can be anchored to the center of the cube in the translation's frame quite easily to a precision of about 0.1 mm by eyesight and contact between the probe and

6

the magnet. However, the tilt of the detector and the refinement of its position related to the cube requires more involved calibration. If one defines the attitude of the detector as shown on Fig. 3a, Eq. (19) can be modified for B_z, as measured by the Hall detector:

$$B_z^{Meas} = \begin{bmatrix} \cos\phi_d \sin\theta_d & \sin\phi_d \sin\theta_d & \cos\theta_d \end{bmatrix} \begin{bmatrix} P_z^X & P_x^Y & P_x^Z \\ P_y^X & P_z^Y & P_y^Z \\ -P_x^X & -P_y^Y & P_z^Z \end{bmatrix} \begin{bmatrix} M_x \\ M_y \\ M_z \end{bmatrix},$$

(20)

One can calibrate the attitude angles through the measurement of the cube in a plane, as stated above, with the cube successively rotated by a known angle Ω around the z axis. In our case, the geometry of a cube makes easy to reliably rotate by $\frac{\pi}{2}$. One then obtains a set of measurement matrices corresponding to each rotation angle. All of these measurements are related to each other by a simple rotation of angle Ω such that the measured B_z verifies:

$$B_z^{Meas} = \begin{bmatrix} \cos\phi_d \sin\theta_d & \sin\phi_d \sin\theta_d & \cos\theta_d \end{bmatrix}$$
$$\times \begin{bmatrix} P_z^X & P_x^Y & P_x^Z \\ P_y^X & P_z^Y & P_y^Z \\ -P_x^X & -P_y^Y & P_z^Z \end{bmatrix} \begin{bmatrix} \cos\Omega & \sin\Omega & 0 \\ -\sin\Omega & \cos\Omega & 0 \\ 0 & 0 & 1 \end{bmatrix} \begin{bmatrix} M_x \\ M_y \\ M_z \end{bmatrix}.$$

(21)

As the cube properties and the detector orientation remain unchanged from one rotation to the other, it is possible to use these measurements to obtain at once the magnetization of the cube, the attitude of the detector, and the center of the cube compared to the position of the detector (if the set of measurements is well conditioned). It can be assumed that the attitude of the detector and the center of the cube are not going to change when switching to the next cube to be measured. As a result, it is possible to measure the entire set of cubes by using only one calibration for one cube in a given orientation. The best possible alignment should nevertheless be achieved before calibration. If the detector is tilted too much or too much off-center, the issue of planar field effect may be encountered.

We present in Fig. 3 histograms of values for the different components of the magnetization of our set of cubes in spherical coordinates for the north pole. We assessed the repeatability of the measurement to 0.5–1% for the magnetization, 0.5° for θ and 2° for ϕ. The difference between the magnetization calculated with the dipole assumption and the cube assumption is about 1.5–2% on the magnetization amplitude, between $-1°$ and $1°$ on θ and a few tens of degrees on ϕ (the precision on the latter quantity is low in any case as θ is close to zero). It seems hence significantly more accurate to use the cube assumption in this case. The observed mean magnetization is 1.38 T with a standard deviation of 0.01 T and the average inclination is 1.8° with standard deviation of 0.9°. This measurement method does not take into account the possible inhomogeneities of magnetization in the parallelepiped, which have a lesser effect.
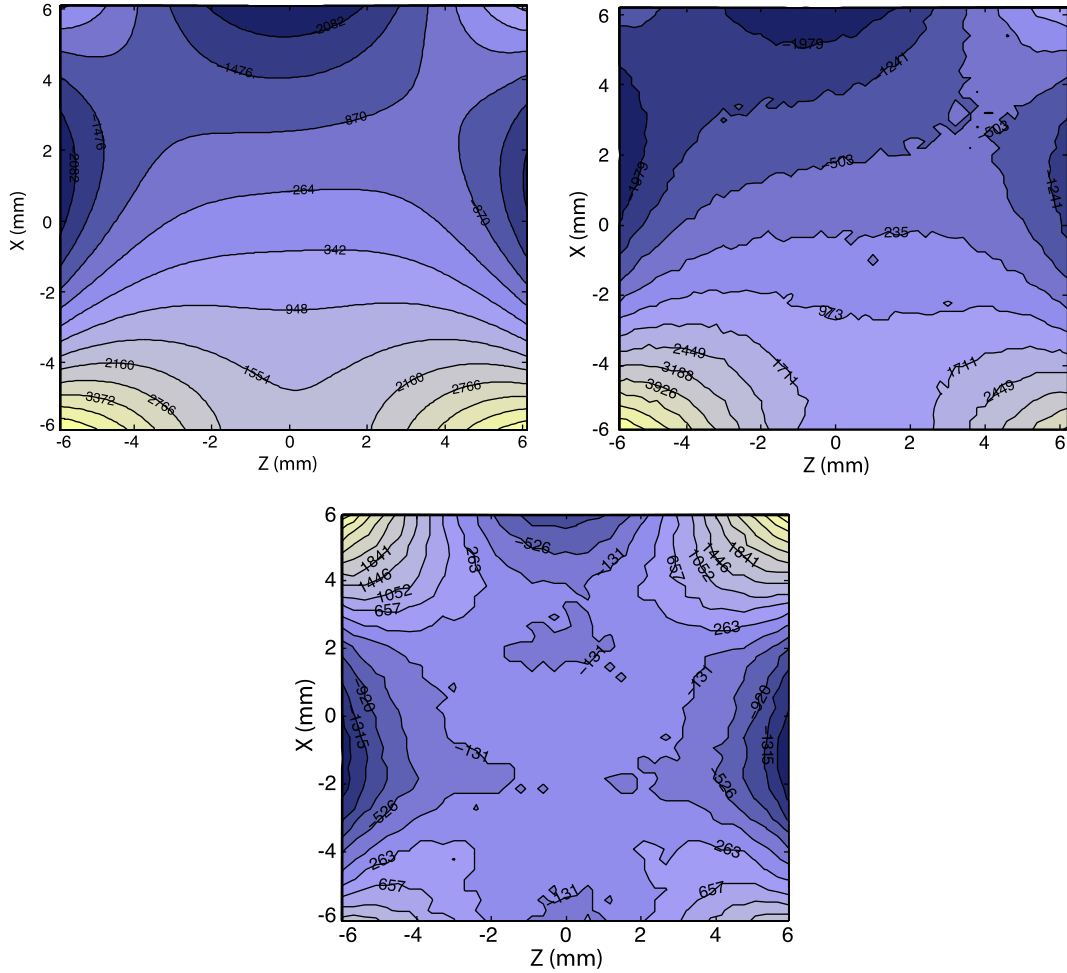

Fig. 4. Contour plots (in ppm) of B_z in the xOz plane for (a) a simulation of the original magnet with Radia based on the measurements of the cubes, (b) the experimental measurements of the original magnet and (c) the experimental measurements of the shimmed magnet. Simulations based on part measurements can give qualitative as well as quantitative information on the field variations. Furthermore, plot (c) shows the shimming using small magnets glued in place at calculated positions provides significant improvement on the field variations.

3.4. Fabrication strategies: simulation based on measurements and screening

The magnetization measurements can be used in first place to skim off the worst pieces which deviate the most from the average values of the set of magnets. The performances of a particular combination of parts can be simulated based on the measurements. In order to perform fast estimations of a combination, we assumed the cubes were simple dipoles for which we derived simple analytical formulae of the spherical harmonic expansion. These formulae allow the quick evaluation of the homogeneity of the magnet in view of massive screening. This dipolar approximation is not inappropriate in this case as this step of fabrication aims at reducing coarse imperfections. Following the notation of Eq. (6), we can write, for example, the Zz_1 and Xz_1^1 terms as

$$Zz_1 = 2\frac{r_0}{R_0}\left[3\cos\theta_1 P_3(\cos\theta_0) + \sin\theta_1 P_3^1(\cos\theta_0)\cos(\phi_1 - \phi_0)\right]$$

$$Xz_1^1 = \frac{r_0}{R_0}\left\{4\cos\theta_1 P_3^1(\cos\theta_0)\cos\phi_0 - 6\sin\theta_1 P_3(\cos\theta_0)\cos\phi_1 \right.$$
$$\left. + \sin\theta_1 P_3^2(\cos\theta_0)\cos(2\phi_0 - \phi_1)\right\}$$

where r_0 is a reference radius, $\{R_0, \theta_0, \phi_0\}$ are the spherical coordinates of the dipole position, and $\{M_1, \theta_1, \phi_1\}$ are the spherical coordinates of the dipole magnetization. The associated Legendre polynomials P_n^m are defined without the $(-1)^m$ Hobson's factor. One can hence estimate the SHE of the magnet simply based on the positions of the cubes and their magnetic measurements. It is possible to rapidly screen thousands of possible combinations in order to refine the layout of the cubes. It is however impossible to span the whole set of combination. The result of such a screening yields a better solution with higher likelihood than when doing it randomly. However, this is not sufficient for the achievement of NMR-grade performances as the knowledge of the magnetization of a magnet is limited to about 1%.

Based on the measurements of the cubes, it is also possible to simulate a given combination with Radia, in order to assess the performance of the magnet. The resulting simulations including demagnetization are accurate with a field at center predicted within 0.2% of the experimental field. We were also able to obtain qualitative and quantitative assessments of the field variations on a large scale. It is possible to predict the coarse variations of the system, which will have to be corrected before starting fine adjustments based on NMR. We present on Fig. 4 the contour plot of B_z in the xOz plane for the simulated magnet and for the experimental measurements using a Hall probe. These results confirm the possibility of estimating quantitatively the performances of the magnet assembly once the cubes have been carefully characterized.

3.5. Characterization of the magnet and correction system

3.5.1. Magnet measurement

Based on the discussion of Section 2.2, we can now have a look at the measurement of the magnet used as an example in this paper. Theoretically, the first non-zero term is Zz_4. This means that the relevant terms to assess the quality of the magnet are all terms up to and including order 3. Higher order terms are bound to be present but should be negligible in the volume of interest (as we will keep the radius small enough to obtain small variations of the order 4). However, we need to perform the measurements on a larger radius for practical reasons (the radius of the volume of interest is only 1.5 mm) and are hence subject to aliasing. As we saw we can reasonably simulate the field, the necessary number of measurement points can be evaluated through simulation. Fig. 5 presents the resulting values of the Zz_n terms for different number of sampling points on a sphere of radius 5 mm. Similar re-
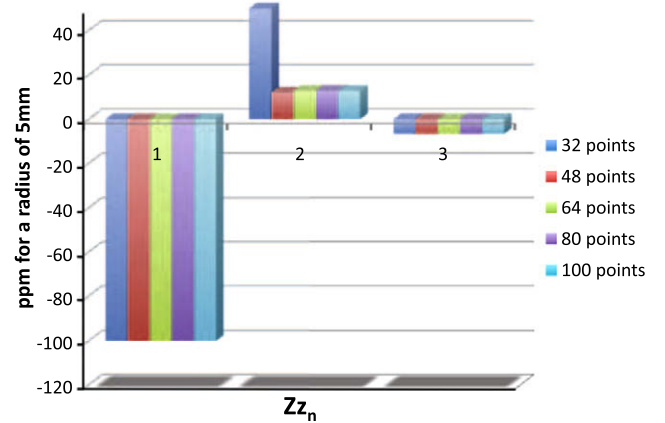

Fig. 5. Simulated measurement of the relevant Zz_n terms for the discussed magnet, with a measurement radius of 5 mm. The stability of the calculated terms with the increase of measurement points indicates spectral folding is not significantly affecting the terms of interest. Similar results can be obtained with the Xz_n^m and Yz_n^m but are not shown here as they do not add information.

sults can be found with the Xz_n^m and Yz_n^m but are not shown here. While 32 points are clearly insufficient (Zz_1 is off by more than 300 ppm), 48 points seem sufficient to achieve a 1 ppm accuracy on all terms. However, using more than 64 points is not useful.

The field mapping measurements in practice can be done with any magnetic field sensor mounted on a positioning system, or with any magnetic field sensor array providing the appropriate measurement locations, as proposed by Metrolab [28]. We use in our laboratory both Hall probes (Lakeshore 3-axis probe with Lakeshore Gaussmeter Model 460) and house-made micro-NMR probes. The positioning system is made of three motorized transla-
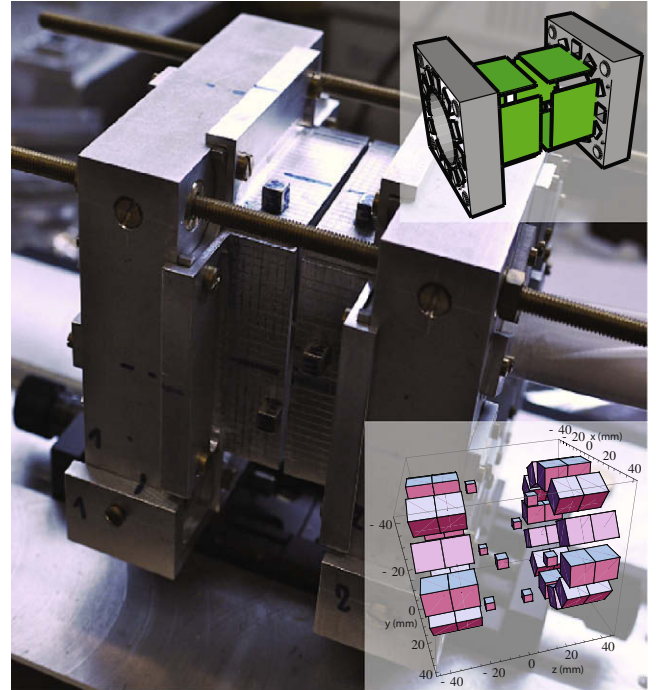

Fig. 6. Photograph of the shimmed magnet. The small magnet cubes can be seen between the two main rings. The upper right schematic shows the four planes where the location of the shims was constrained. The lower right schematic shows a 3D view of the magnetic elements of the system. Our method allows the fabrication of a shimmed magnet with a field strength very close to the theoretical one (about 2% difference).

8

tional stages (stages Newport model 443 with 50 mm travel distance coupled with motors LTA-HS). This system offers positioning with an accuracy better than 10 μm. We developed a LabView software to synchronize motion and measurements both with the Gaussmeter and the NMR spectrometer (Tecmag Apollo) in order to automate the measurement procedure. This equipment provides us the ability to perform measurements with arbitrary schemes in order to extract the SHE terms, which are the basis of the shimming procedure necessary to compensate the magnet imperfections.

3.5.2. Correction system

Some high performance magnets have been proposed in the past [29,14], based on intrinsically inhomogeneous structures (due to geometry) corrected by motion of significant additional magnet blocks. Here, however, we start with a magnet theoretically homogeneous to an arbitrary order. The inhomogeneities are hence mainly due to material imperfections and scarcely to geometry. This results in a reduced need in shims. One can afford the use of very small shim pieces to correct for the imperfections of the magnet. Adding small pieces of ferromagnetic material to the magnet in order to compensate its inhomogeneities is a standard procedure in MRI [30,31] and was further developed for

permanent magnets [32]. We adapted this method to serve our purpose in this example.

The correction of our simple example magnet can be done by using small magnet cubes placed at appropriate locations. The full correction of the magnet, meaning up to the theoretical homogeneity, necessitates the cancellation of fifteen terms ($Z_1, Z_2, Z_3, X_1^1, Y_1^1, X_2^1, X_2^2, Y_2^1, Y_2^2, X_3^1, X_3^2, X_3^3, Y_3^1, Y_3^2, Y_3^3$). One needs $p + 1$ independent parameters to cancel p terms. As a result, we need at least 16 parameters. A single cube features three translational degrees of freedom and three rotational degrees of freedom. We decided to set the orientation of each cube to the most efficient orientation given their location, i.e. antiparallel to the field at the center of the magnet, leaving no rotational degrees of freedom. For ease of realization, we require to tie the possible positions of each cube to a plane. As a result, only two translational degrees of freedom remain for each cube. It follows that one needs at least 8 cubes in order to cancel all undesired terms and achieve theoretical homogeneity. The symmetries of the magnet lead to place each
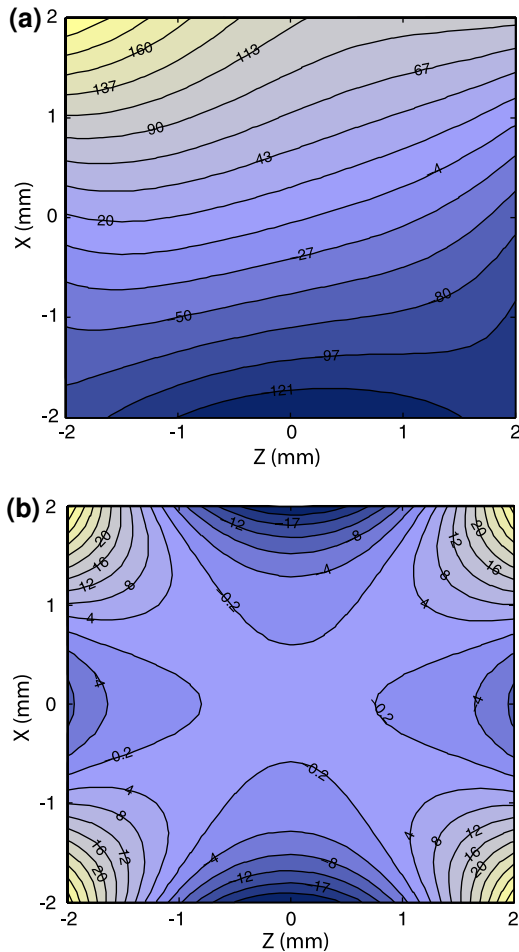

Fig. 7. Contour plots of B_z (in ppm) in the xOz plane for (a) a simulation of the unshimmed magnet with Radia based on imperfect cubes, and (b) for a simulation of the same magnet shimmed with small cubes. The position of each shim cube has been calculated in order to minimize the different terms in the spherical harmonics expansion. One can observe the dramatic improvement of the field homogeneity after shimming.
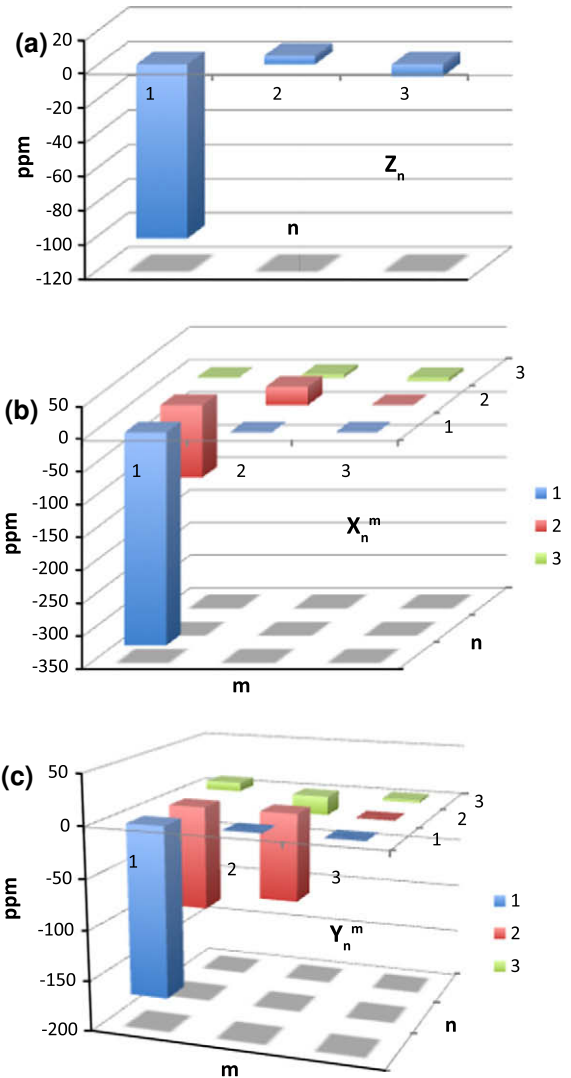

Fig. 8. Contribution of the different orders to the field variations on a sphere of radius 5 mm for a magnet with perfect geometry using the measured cubes. Only terms theoretically cancelled are shown. (a) Bar graph of the axial orders contributions. One can notice the cancellation of Z_2 due to the appropriate gap adjustment. The gradient Z_1 is the dominant term and Z_3 is in this case very small. (b) and (c) Bar graphs of the different skewed terms X_n^m and Y_n^m. The gradient term X_1^1 and Y_1^1 are dominant but an order of magnitude smaller than in the low-cost solution. Second order skewed terms are also very noticable.
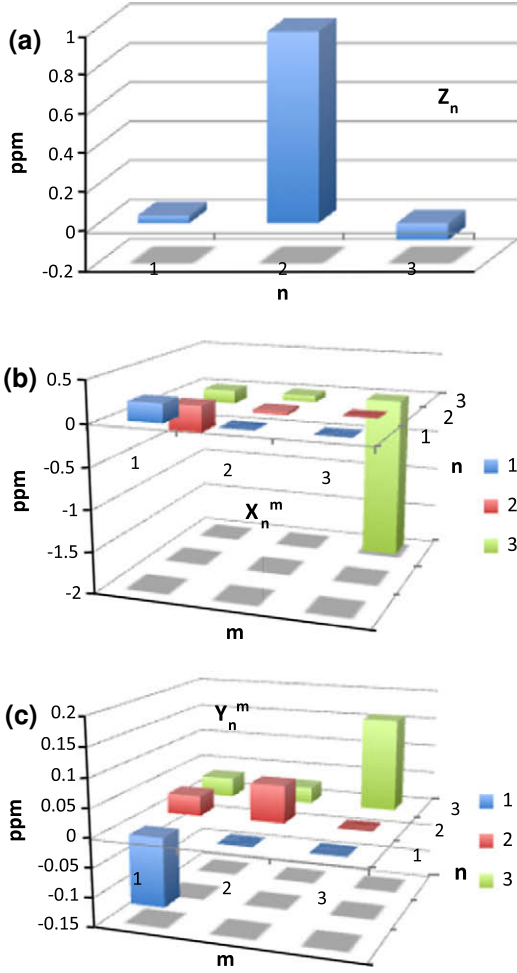
Fig. 9. Contribution of the different orders to the field variations on a sphere of radius 5 mm for a magnet with perfect geometry using the measured cubes. The magnet is shimmed by small cubes as shown on Fig. 6 using the method described in the text. Only terms theoretically cancelled are shown. (a) Bar graph of the axial orders contributions. One can notice all terms are reduce to a sub-ppm contribution and the Z_2 term now dominates the axial terms. The remaining variations are due to the error made by the dipolar approximation. (b) and (c) Bar graphs of the different skewed terms X_n^m and Y_n^m. All terms are reduced to less than 2 ppm. The Y_n^m terms are especially well corrected, remaining below 0.2 ppm in absolute value. The whole system is dominated by X_3^3. This remaining term is also due to the error made with the dipolar approximation of the shims. However, this could be refined through the use of an additional set of small cubes placed further away from the magnet system center.

cube in a quadrant of the *xOy* plane, symmetrically in regard of that same plane. The areas where each shimming cube can be placed are shown on Fig. 6.

It is of course necessary to verify that the variables offered by the shimming system can span the relevant part of the expansion. We hence conducted a theoretical study of such a shimming scheme. Based on the measurements of the cubes constituting the magnet, we simulated the magnet inhomogeneities using Radia, in order to include demagnetization. The measurement scheme was simulated numerically and the extraction algorithm was used in order to obtain simulated SHE terms. Based on these simulations, we computed the appropriate position of the shimming cubes and added them to the Radia simulation. The shimmed magnet is shown on Fig. 6 and the field profiles before and after shimming are shown on Fig. 7. Figs. 8 and 9 present the values of the different terms before and after shimming. The results are close to perfect and very encouraging for proceeding with the procedure experimentally.
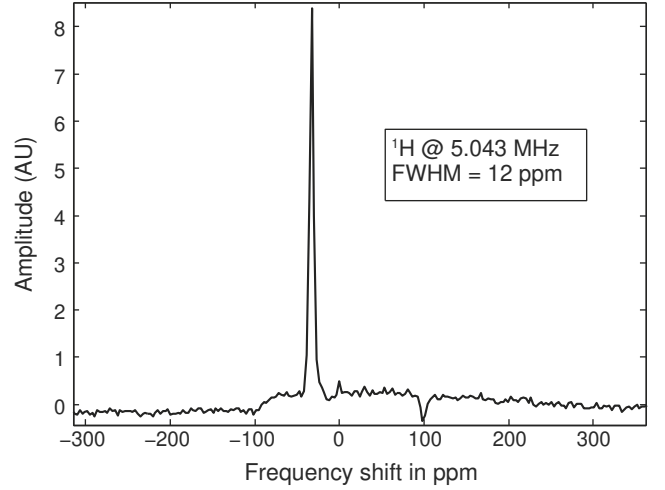

Fig. 10. ^{1}H NMR spectrum of a 3 mm^3 sample of water (doped with CuSO$_4$) in the shimmed magnet. The achieved full width at half maximum is about 12 ppm, displaying a major improvement on the original 40 ppm linewidth obtained with the same magnet unshimmed.

The compensation of the magnet can also be done through modifications of its geometry. It is possible to have some play on the gap between the rings of the magnet and also on the orientation of each ring relative to the other. These geometry modifications are of course very sensitive and have a great impact on the field variations at the center. The terms mainly concerned by such movements are the different gradients Zz_1, Xz_1^1, Yz_1^1 and Zz_2.

We applied this shimming scheme using Hall probe measurements. We successfully obtained the SHE terms and computed the necessary positions of the shimming cubes (previously characterized). This resulted in a great improvement of the homogeneity, as it can be seen on Fig. 4c. The NMR linewidth was improved from 40 ppm [23] to 12 ppm (see Fig. 10) for a sample of 3 mm^3. The sequence used was a simple $\frac{\pi}{2}$-acquisition featuring 512 points with a dwell time of 130 μs. The acquisition was done at 5.04 MHz in 128 scans (25.6 s) on a sample of water doped with CuSO$_4$. This result is not as good as the 5 ppm the theory lets us expect for the same sample size, but it can be explained by the crude positioning of the shims in this prototype (precision on the location of the shims of about 0.5 mm).

4. Discussion and conclusions

We described a detailed method to design theoretically homogeneous magnets up to an arbitrary order. This method is based on the spherical harmonics, which have been used in the field of electromagnet design for a long time but scarcely for permanent magnet systems. This very systematic method can transform the design of a magnet into a Lego game, once one has the appropriate analytical formulas. The attainable homogeneity has in theory no limitations, provided enough elements are used. Following these concepts, we built a simple example of magnet which is very light-weighted (1.8 kg), low-cost (100 euros in magnets) and provides an easy access while delivering ~120 mT (5.1 MHz proton) along the axis. We present an assembly method based on the characterization of the individual cubes constituting the magnet and complete this assembly method with a shimming methodology which successfully achieved a homogeneity close to the theoretical while using a minimum quantity of shimming material and number of iterations. The shimming procedure relies on the measurement of the spherical harmonic expansion terms of the field for which we discussed practical aspects including some usually

dismissed accuracy considerations. We hence were able to obtain a magnet with a field profile close to the one theoretically calculated. The line width of a 3 mm^3 water sample is about 12 ppm. This performance is, as expected from the theory (6 ppm in the same volume), not as good as what was obtained in some existing systems which also took advantage of bigger magnet size or smaller sample size and stronger field. However, this example gives a preview of the possibilities offered by using an analytically perfect starting point for the fabrication. The theoretically perfect structure is perturbed by material and geometrical imperfections which can be corrected by small perturbations of the original design. It is then possible to take the structure to the best of its capabilities.

Another benefit of permanent magnets is that the obtained solution is scalable. The system can be rendered as small (or as large) as needed, the field strength and homogeneity properties will not change, besides the gradient (which is also scaled). Furthermore, this study opens the road to more involved designs for highly homogeneous *ex situ* and *in situ* magnets. Moving towards more homogeneous systems will require the use of more rings with appropriate dimensions as more terms of the expansions will have to be cancelled. Finally, this method is also valid for transverse and arbitrary oriented fields and makes possible the design of homogeneous systems with the field directly at the magic angle for magic angle field turning [33]. In that sense, this small prototype is a major step toward such a magnet as a longitudinal component of the field will be required.

Acknowledgments

References

[1] D.E. Woessner, The early days of NMR in the Southwest, Conc. Magn. Reson. 13 (2) (2001) 77–102.
[2] R.H. Varian, Apparatus and method for identifying substances, US Patent 3,395,337, July 1968.
[3] M. Sagawa, S. Fujimura, H. Yamamoto, Y. Matsuura, Permanent magnet materials based on the rare earth–iron–boron tetragonal compounds, IEEE Trans. Magn. MAG-20 (5) (1984) 1584–1589.
[4] K. Halbach, Design of permanent multipole magnets with oriented rare earth cobalt material, Nucl. Instrum. Methods (69) (1980) 1–10.
[5] G. Eidmann, R. Savelsberg, P. Blümler, B. Blümich, The NMR MOUSE, a mobile universal surface explorer, J. Magn. Reson. A 122 (1996) 104–109.
[6] H. Raich, P. Blümler, Design and construction of a dipolar Halbach Array with a homogeneous field from identical bar magnets: NMR mandhalas, Conc. Magn. Reson. 23B (1) (2004) 16–25.
[7] S. Rahmatallah, Y. Li, H.C. Seton, I.S. Mackenzie, J.S. Gregory, R.M. Aspden, NMR detection and one-dimensional imaging using the inhomogeneous magnetic field of a portable single-sided magnet, J. Magn. Reson. 173 (2005) 23–28.
[8] A.E. Marble, I.V. Mastikhin, B.G. Colpitts, B.J. Balcom, An analytical methodology for magnetic field control in unilateral nmr, J. Magn. Reson. 174 (2005) 78–87.
[9] B. Manz, A. Coy, R. Dykstra, C.D. Eccles, M.W. Hunter, B.J. Parkinson, P.T. Callaghan, A mobile one-sided NMR sensor with a homogeneous magnetic field: the NMR-MOLE, J. Magn. Reson. 183 (2006) 25–31.
[10] A.E. Marble, I.V. Mastikhin, B.G. Colpitts, B.J. Balcom, A constant gradient unilateral magnet for near-surface MRI profiling, J. Magn. Reson. 183 (2006) 228–234.
[11] B. Blümich, J. Perlo, F. Casanova, Mobile single-sided NMR, Prog. Nucl. Magn. Reson. Spectrosc. 52 (2008) 197–269.
[12] J.L. Paulsen, L.S. Bouchard, D. Graziani, B. Blümich, A. Pines, Volume-selective magnetic resonance imaging using an adjustable, single-sided, portable sensor, PNAS 105 (52) (2008) 20601–20604.
[13] A. McDowell, E. Fukushima, Ultracompact NMR: ^{1}H spectroscopy in a subkilogram magnet, Appl. Magn. Reson. 35 (2008) 185–195.
[14] E. Danieli, J. Mauler, J. Perlo, B. Blümich, F. Casanova, Mobile sensor for high resolution NMR spectroscopy and imaging, J. Magn. Reson. 198 (2009) 80–87.
[15] F. Roméo, D.I. Hoult, Magnet field profiling: analysis and correcting coil design, Magn. Reson. Med. 1 (1984) 44–65.
[16] G. Aubert, Cylindrical permanent magnet with longitudinal induced field, US Patent 5,014,032.
[17] G. Aubert, Cylindrical permanent magnet to produce a transversal and uniform induction field, US Patent 4,999,600.
[18] A.E. Marble, I.V. Mastikhin, B.G. Colpitts, B.J. Balcom, Designing static fields for unilateral magnetic resonance by a scalar potential approach, IEEE Trans. Magn. 43 (5) (2007) 1903–1911.
[19] J.D. Jackson, Classical Electrodynamics, third ed., Wiley, 2002.
[20] P.C.M.V. Zijl, S. Sukumar, M.O. Johnson, P. Webb, R.E. Hurd, Optimized shimming for high-resolution nmr using three-dimensional image-based field mapping, J. Magn. Reson., Ser. A 111 (2) (1994) 203–207.
[21] R.W. Hamming, Numerical Methods for Scientists and Engineers, Dover Publications, 1987.
[22] J.R. Higgins, Sampling Theory in Fourier and Signal Analysis. Foundations, Oxford Science Publications, 1996.
[23] C. Hugon, P.M. Aguiar, G. Aubert, D. Sakellariou, Design, Fabrication and Evaluation of a Low-Cost Homogeneous Portable Permanent Magnet for NMR and MRI, C.R. Chimie, 2010, in press.
[24] P. Elleaume, O. Chubar, J. Chavanne, Computing 3D magnetic fields from insertion devices, in: Proceedings of the PAC97 Conference, 1997, pp. 3509–3511.
[25] R.S. Popovic, Hall Effect Devices, Institute of Physics, 2004.
[26] H. Onuki, P. Elleaume, Undulators, Wigglers and their Applications, CRC Press, 2003.
[27] M. McCaig, A.G. Clegg, Permanent Magnets in Theory and Practice, second ed., Pentech Press, 1987.
[28] Metrolab Instruments SA, 110, ch. Du Pont-du-Centenaire, CH1228 Geneva, Switzerland, MFC-3045 magnetic field camera, March 2004.
[29] J. Perlo, F. Casanova, B. Blümich, Ex situ NMR in highly homogeneous fields: ^{1}H spectroscopy, Science 315 (2007) 1110–1112.
[30] D. Hoult, D. Lee, Shimming a superconducting nuclear magnetic resonance imaging magnet with steel, Rev. Sci. Instrum. 56 (1) (1985) 131–135.
[31] A. Belov, V. Bushuev, M. Emelianov, V. Eregin, Y. Severgin, S. Sytchevski, V. Vasiliev, Passive shimming of the superconducting magnet for MRI, IEEE Trans. Appl. Supercond. 5 (2) (1995) 679–681.
[32] G. Aubert, US Patent 4,835,504, 1989.
[33] D. Sakellariou, C.A. Meriles, R.W. Martin, A. Pines, NMR in rotating magnetic fields: magic-angle field spinning, Magn. Reson. Imag. 23 (2005) 295–299.